



## Article

# Study of Atomic Oxygen Airglow Intensities and Air Temperature near Mesopause Obtained by Ground-Based and Satellite Instruments above Baikal Natural Territory

Andrei Saunkin <sup>\*</sup>, Roman Vasilyev and Olga Zorkaltseva 

Institute of Solar-Terrestrial Physics SB RAS, 664033 Irkutsk, Russia; roman\_vasilyev@iszf.irk.ru (R.V.); meteorologist-ka@yandex.ru (O.Z.)

<sup>\*</sup> Correspondence: saunkin@iszf.irk.ru

**Abstract:** The research studied the comparison of the night air temperatures and the atomic oxygen airglow intensities at the mesopause obtained with satellite and ground-based instruments. Satellite data used in this study were obtained with the SABER limb-scanning radiometer operating aboard the TIMED satellite. Data of ground-based monitoring were obtained using the KEO Scientific “Arinae” Fabry–Pérot interferometer adapted for aeronomic research. Since an interferometer detects parameters of the 557.7 nm line for the entire emission layer, it is not quite appropriate to perform a direct comparison between the upper atmospheric temperature obtained from ground-based observations and that from a satellite at a particular height. To compare temperatures correctly, the effective temperature must be calculated based on satellite data. The effective temperature is a height-averaged temperature profile with the weight factors equal to the 557.7 nm line intensity at relevant heights. The height profile of intensity of this natural green airglow of the upper atmosphere is calculated from the height profile of atomic oxygen concentration. Data on chemical composition and air temperature at the mesopause from SABER were used to calculate the profiles. The night intensity of the 557.7 nm emission obtained from satellite data in this way was in good accordance with the results of ground-based observations, but the temperatures were different. The reason for temperature discrepancy was assumed to lie in the incorrect position of the intensity maximum of the reconstructed emission layer. According to our calculations based on SABER data, the intensity peak was observed at the height of 94–95 km. By shifting it relative to the SABER temperature height profile, we re-calculated the effective temperatures and compared them with the interferometer data. The best coincidence between seasonal temperature variations obtained using the proposed method was achieved when the maximum of the reconstructed 557.7 nm intensity height profile was shifted to 97 km, but it could not eliminate minor local differences in temperature behavior.

**Keywords:** SABER TIMED; Fabry–Pérot interferometer; airglow; line 557.7 nm; mesosphere temperature



**Citation:** Saunkin, A.; Vasilyev, R.; Zorkaltseva, O. Study of Atomic Oxygen Airglow Intensities and Air Temperature near Mesopause Obtained by Ground-Based and Satellite Instruments above Baikal Natural Territory. *Remote Sens.* **2022**, *14*, 112. <https://doi.org/10.3390/rs14010112>

Academic Editor: Simone Lolli

Received: 25 November 2021

Accepted: 24 December 2021

Published: 28 December 2021

**Publisher’s Note:** MDPI stays neutral with regard to jurisdictional claims in published maps and institutional affiliations.



**Copyright:** © 2021 by the authors. Licensee MDPI, Basel, Switzerland. This article is an open access article distributed under the terms and conditions of the Creative Commons Attribution (CC BY) license (<https://creativecommons.org/licenses/by/4.0/>).

## 1. Introduction

Comparison of atmospheric parameters observed with ground-based and satellite instruments is important to study the Earth’s atmosphere, especially the upper atmosphere in particular (mesosphere, lower thermosphere), where direct observations of temperature, composition, wind speed, etc. are hampered and quite rarely conducted using geophysical rockets. On the one hand, such comparisons allow verifying the methods of remote indirect observation of atmospheric parameters, while on the other hand, they offer additional opportunities for a more detailed investigation into physical and chemical processes in the atmosphere. For example, article [1] describes air density correction in the NRLMSISE-00 empirical model. The correction is based on data obtained using the SABER instrument aboard the TIMED satellite. The performed correction results in far better accuracy of the model at 80–100 km. In [2], the authors compared spatial distributions of the hydroxyl

airglow intensity and air temperature obtained using the special all-sky imaging system at Ranchi station in India (23.3°N, 85.3°E) and temperatures obtained with SABER above this location. The results of the experiment are consistent, and the dispersions of the values obtained are within admissible limits. The article [3] compares the mesopause temperature at the height of hydroxyl emission detected with the ground-based infrared spectrograph at the mid-latitude Maimaga station in Yakutsk and the mesopause temperature obtained with the SABER satellite in the same region. In [4], too, comparative analysis of temperature was performed using the high-latitude ground-based spectrometer SATI (Spectral Airglow Temperature Imager) in Sierra Nevada, Spain, and the SABER satellite instrument. In turn, ref. [5] compared several instruments and calculated shifts in temperatures measured with the ground-based Davis spectrometer in the Antarctic and those obtained from the Aura/MLS and TIMED/SABER satellite data. The article [6] discusses the optimal choice of Einstein coefficients to determine the rotational temperature using a spectrometer (Horiba model: IHR550) in Xinglong China (40°24'N, 117°35'E) and SABER data. Conclusions put forth in all the listed works denote fairly good correspondence between data obtained with satellite and ground-based instrumentation. The airglow of the 557.7 nm atomic oxygen line occurs near the mesopause region, a little higher than the hydroxyl airglow. There exists a potential for temperature and wind observations by analyzing the 557.7 nm line Doppler broadening and shifting using aeronomic Fabry–Pérot interferometers that operate in high latitudes [7,8]. However, no comparison has been conducted with satellite data for such devices. This is important both to check the performance of the method for ground-based observation of the Earth's upper atmosphere parameters and to refine features of dynamics of the upper atmosphere parameters at the mesopause at the mid-latitudes of Eurasia. Ground-based instruments have a better time resolution in comparison with the satellite-borne devices. Therefore, the importance of the ground-based instruments for studying the tides internal gravity waves and other processes that require time resolution in minutes and tens of minutes is obvious. Thus, in our study, we assessed the extent of compliance between the data from ground-based (Fabry–Pérot interferometer) and satellite (limb-scanning radiometer) measurements of the upper atmosphere temperature. The intensity of the 557.7 nm atmospheric airglow line recorded with ground-based equipment resulted from the atomic oxygen ( $^1S$ )–( $^1D$ ) transition at the height of 90–100 km. Height profiles of the upper atmosphere physical and chemical parameters (including temperature) were considered in the same range of heights using satellite limb-scanning radiometry.

## 2. Data and Methods

### 2.1. Observational Facilities and Initial Data

The KEO Scientific «Arinae» Fabry–Pérot interferometer (FPI) selected as the ground-based instrument for temperature observations in the upper atmosphere is located in the ISTP SB RAS Geophysical Observatory near the settlement of Tory (Russia, Buryat Republic). The principle of temperature detection is based on recording the Doppler broadening of the 557.7 nm line of natural night atmospheric glow emitted by atomic oxygen in the layer ~10 km thick located at 90–100 km above the Earth's surface. A detailed description of the interferometer, the algorithm of its operation, and the method of data processing to detect temperature can be found in [9,10]. The lack of a calibration light source on the wavelength close to that of 557.7 atomic oxygen airglow leads to some distortions of the temperature obtained based on this technique; therefore, the instrument was primarily calibrated according to satellite data using the algorithm put forth in [11]. The idea was to minimize the difference in seasonal variations of temperatures observed by FPI  $T_{FPI}(t)$  and seasonal variations of temperatures observed by SABER at selected height  $T_{SABER}(t, h)$ . We vary height and coefficients of linear dependence— $T(t)_{FPI} = aT_{FPIobs}(t) + bw$ ; here,  $T_{FPIobs}(t)$  is observed biased temperatures to minimize  $E = \sum_t (T_{SABER}(t, h) - T(t))^2$ . The values of  $a$  and  $b$  obtained in [11] are 0.99 and  $-120$ , correspondingly.

The parameters found resulted in reasonable temperatures and O ( $^1S$ ) emission height. Later, corrected FPI data were compared to the dynamics of the lower atmosphere and

showed the reliable presence of response to sudden stratospheric warming [12,13]. As we did not take into account the height profile of emission in our previous research, now we could try to explain distortions using that additional info.

The satellite instrument used in the study is the SABER limb-scanning radiometer aboard the TIMED satellite [14]. SABER conducts global measurements of atmospheric parameters using a 10-channel broadband infrared radiometer by scanning the Earth's limb and covers the spectral range from 1.27 to 17  $\mu\text{m}$ . These measurements allow obtaining vertical profiles of the following parameters: kinetic temperature, pressure, geopotential height, atmosphere density, volume mixing ratio  $O_3$ , and emission intensity for 2.1  $\mu\text{m}$  OH, 1.6  $\mu\text{m}$  OH, and 1.27  $\mu\text{m}$   $O_2$ . We used data from version 2.0 with sub-version (SABER\_L2A\_20XXXXX\_XXXXX\_02.0.nc) one since, currently, it assures the maximum possible time overlapping of data from ground-based and satellite instruments.

To compare temperature obtained with the satellite and ground-based instruments, it is essential to select the time points when both instruments observed the same volume of the atmosphere. SABER conducts limb measurements and obtains a temperature height profile globally. For comparison, we selected the points in time when the satellite was conducting observations in the area 1400 km in diameter over Baikal natural territory, with the geophysical observatory in Tory being in the center. In addition, since FPI observations are basically performed at night, for our analysis we chose SABER profiles obtained with the 159 to 75 degrees solar angle relative to the horizon (SABER data were collected and spatial filtration was conducted using the information technique and methods developed in the frame of the project "Fundamentals, methods and technologies for digital monitoring and forecasting of the environmental situation on the Baikal natural territory". The project aimed to build a complex dataset including natural, social, technological, etc. information in the region of unique lake Baikal <http://baikal-project.icc.ru/> (accessed on 24 November 2021)).

Figure 1 shows the behavior of the height profile of the middle atmosphere night temperature obtained with SABER within several years above the GPO in Tory. From satellite data, the mesopause position varies in height with an amplitude of  $\sim 13$  km during a year (98 km in winter and 85 km in summer). The mesopause temperature also varies over a year with  $\sim 30$  °K amplitude (145 °K in summer, and 175 °K in winter). A theoretical explanation of the physical and chemical changes in the atmosphere over time can be found in [15].

Actually, there are two basic mechanisms of 557.7 nm light production in the Earth's atmosphere. First and most bright is the aurora initiated by the precipitated electrons at the polar latitudes during geomagnetic storms. The upper atmosphere processes result in an increase in the air temperature; moreover, the shape of the 557.7 nm line can be distorted during the auroral process, resulting in a wrong temperature estimation [16]. The green aurora intensity at the FPI installation place appears only during the strongest geomagnetic storms [17,18]. We performed our study during quiet geomagnetic years between 2016 and 2020. This was a period of decreasing and minima of solar and geomagnetic activity, so the contribution of the 557.7 nm light from auroral processes could be neglected. A second mechanism was based on the chemical reactions involving atomic oxygen. This mechanism dominated the production of the 557.7 nm airglow near FPI in our research. Details of the second mechanism are described in Section 2.2.

It is universally accepted that the peak height of the 557.7 nm atomic oxygen line airglow is at 95–97 km [17,19]. Seasonal variations in temperature averaged in this observed range of heights from SABER data are weak in contrast to quite strong seasonal temperature variations in the mesopause region according to FPI in Figure 2.

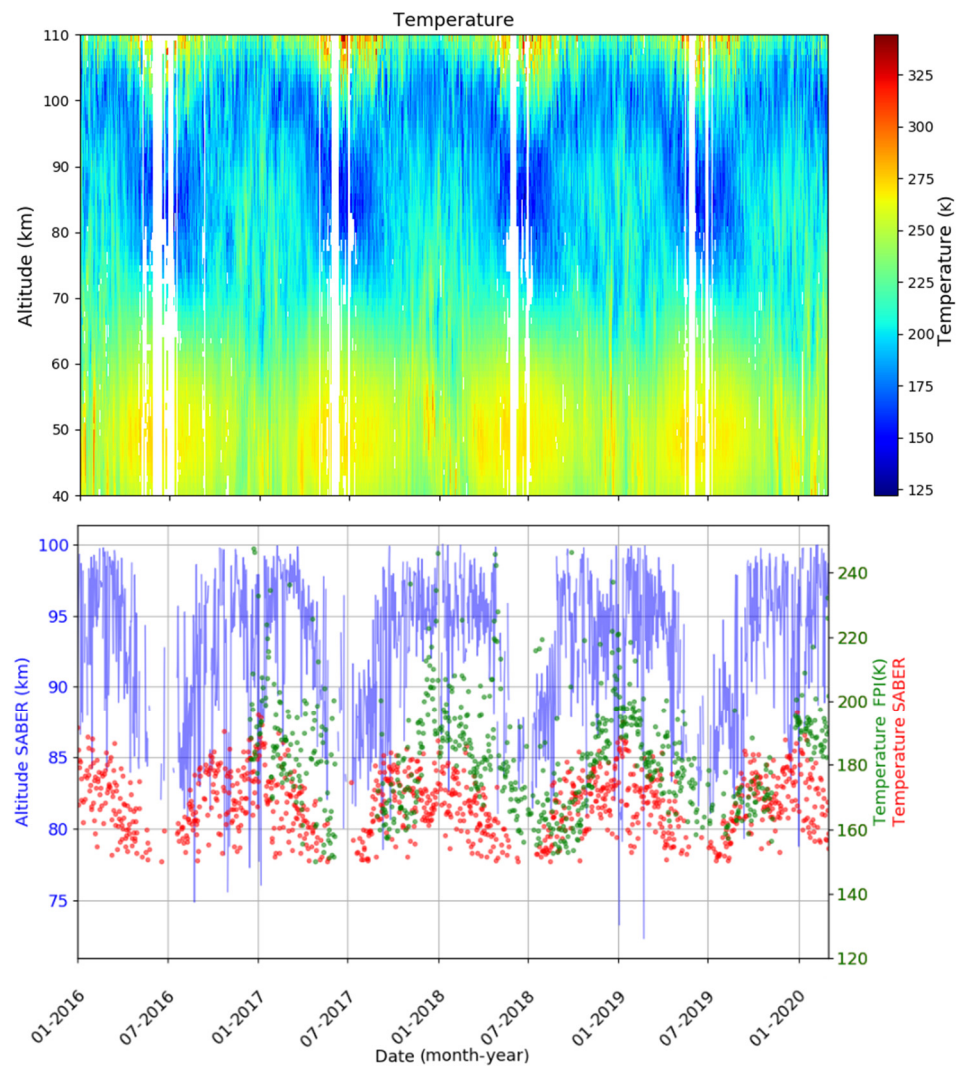


**Figure 1.** Top—behavior of temperature height profile above the GPO in Tory from SABER data. Bottom—variations in the mesopause height (blue line) and temperature obtained from SABER data at an altitude 94 km (red points) and temperature from FPI data (green points). The presented data cover the 2016–2020 time interval.

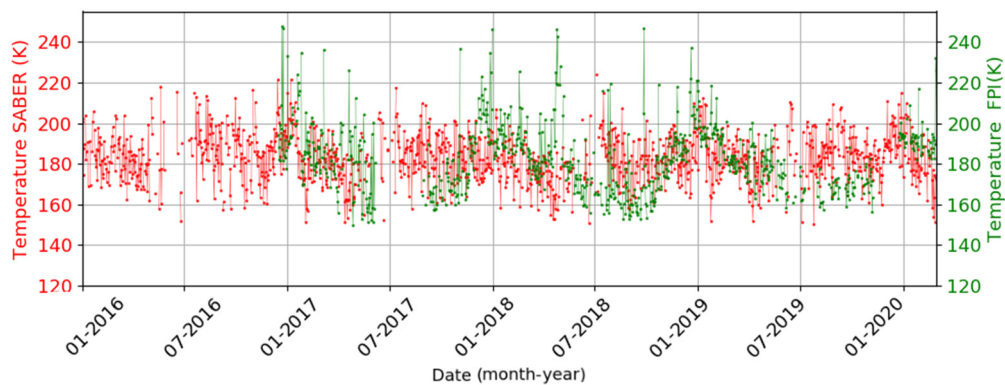


**Figure 2.** Red points—temperature averaged over the 95–97 km heights according to SABER data and above GPO in Tory. Green points—temperature obtained with Fabry–Pérot interferometer in GPO, Tory.

This discrepancy in the results of temperature observations with ground-based and satellite instruments can be explained by the features related to the change in parameters of the height profile of the 557.7 nm atomic oxygen line. Since the FPI registers the integral intensity emitted in a range of heights, the FPI-observed temperature is also an integral characteristic. It can be referred to as the effective temperature resulting from temperature averaging in a height range within the airglow layer with the weights equal to airglow intensity at a certain height:

$$T_{eff} = \frac{\sum_h T(h) \cdot V_{558}(h)}{\sum_h V_{558}(h)} \quad (1)$$

The same approach was undertaken in [6], where the temperature obtained at the ground using hydroxyl airglow was compared with the temperature obtained by SABER.

When we extract essential physical and chemical atmospheric parameters from the profiles of atmospheric characteristics registered with SABER in the specified spatial region near FPI, we can assess the 557.7 nm line airglow profile. Then, we can calculate the profile integrated intensity and effective temperature in order to make a meaningful comparison of data from ground-based and satellite instruments. A similar procedure was performed in [6].

## 2.2. The Method of 557.7 Airglow Reconstruction from SABER Data

To calculate the integral airglow intensity and the effective temperature, reconstruction of the atomic oxygen [O] concentration from the SABER satellite data is required. For this, one can use the technique described in [20], which is based on analyzing SABER data on hydroxyl emission. After that, one can obtain the height profile of the 557.7 nm line airglow intensity (volume emission rate, VER) based on data presented in [21], which describes the method of atomic oxygen calculation from the known 557.7 nm line intensity.

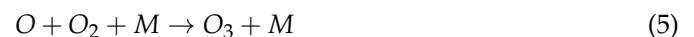
The green line emission at the 557.7 nm wavelength resulting from the  $O$  transition  $O(^1S-^1D)$  is one of the brightest components of the night airglow of the mesosphere. An explanation of the production of an excited oxygen atom  $O(^1S)$  was first proposed by Chapman in terms of three-body recombination of  $O$  atoms [22]. However, the two-step mechanism involving the excited state of  $O_2$  was later proposed by Barth. Studies of the green line and  $O$  atoms by various measurements have generally favored the Barth mechanism [21]. The excited atom of oxygen  $O(^1S)$  with the 4.2 eV energy results from triple collisions with the participation of atomic oxygen (the Barth mechanism) and includes the following stages:



Additionally, the hydroxyl airglow is related to the atomic oxygen chemistry via ozone by reaction:



In this case, ozone is generated from oxygen atoms by means of triple collisions:



Thus, measurements of the hydroxyl airglow parameters can also provide information on the atomic oxygen concentration.

To determine the atomic oxygen concentration at nighttime using the hydroxyl airglow, ref. [20] assumed that ozone production by recombination (Equation (5)) is balanced by its loss resulting from reaction with the atomic hydrogen (Equation (4)). Therefore, the hydroxyl emission intensity observed with the SABER instrument, for instance, is directly proportional to the rate of its formation, and hence, directly proportional to the atomic

oxygen concentration. To calculate the atomic oxygen concentration, ref. [20] introduced a formula where the SABER-measured hydroxyl intensity is determined as follows:

$$= P \left[ \frac{f_9}{A_9 + C_9} A_{97} + \frac{f_8}{A_8 + C_8} A_{86} + \frac{f_9}{A_9 + C_9} \frac{A_{98} + C_{98}}{A_8 + C_8} A_{86} \right] \quad (6)$$

where  $V$  is the observed intensity of hydroxyl volume emission rate, and  $P$  is the rate of hydroxyl production. The latter is set equal to the rate of ozone production, which, in turn, allows obtaining the atomic oxygen following the technique described in [23]. Equation (6) can be reduced to a square equation of atomic oxygen concentration with coefficients containing the SABER-observed intensity of hydroxyl airglow, as well as kinetic and spectroscopic parameters, whose values are presented in [20]. However, in the latest article [24] there was given new coefficients for Equation (6), and in our work, we show results for both versions.

Figure 3 presents height profiles from satellite data of ozone relative concentration (mixing ratio) (a), the hydroxyl airglow intensity (b), and the atmosphere density (c) (logarithmic scale) over 2016–2019. In the profiles, temperature height profiles from SABER data are shown in red. The profiles were obtained for the local time nearest to midnight in the addressed spatial area.

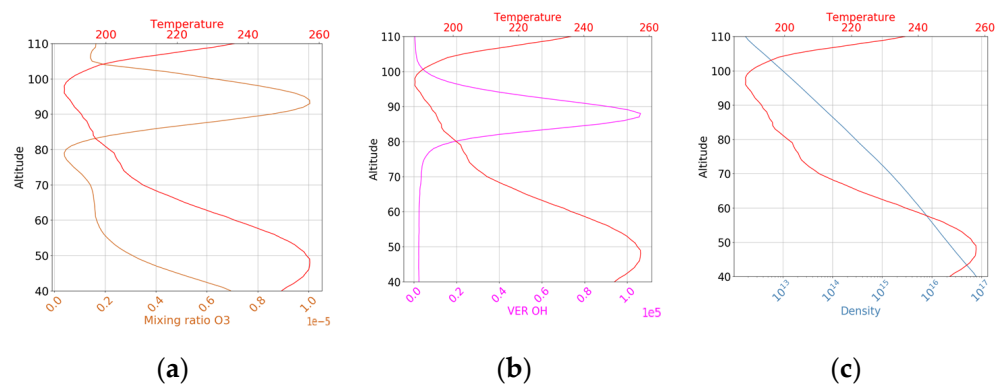


**Figure 3.** (a) Vertical profile of ozone mixing ratio, (b) hydroxyl  $\frac{\text{erg}}{\text{cm}^3/\text{s}}$ , and (c) the atmospheric density [ $\text{cm}^{-3}$ ], (logarithmic scale).

Figure 4 presents the atomic oxygen concentration height profiles averaged over the considered time interval, which were obtained using the above technique for both versions of coefficients. The blue profile is the result obtained with the coefficients taken from [20], and the red line profile represents the result by using the new coefficients from [24]. Comparing these two profiles it was discovered that by using new coefficients the maximum of atomic oxygen concentration is at the height  $\sim 95$  km—it is about 1 km higher than using the old coefficients. The concentration of atomic oxygen becomes remarkably higher over 93–100 km. However, the resulting number of obtained height profiles of concentration of atomic oxygen using Equation (6) with the new coefficients is smaller than using the old version of coefficients (see Figure 5). The variance of the concentration in new datasets also increases, so the red line profile is not as smooth as the blue one. Additionally, we can note a sharp increase in the atomic oxygen concentration in the upper part of the profiles. In the articles serving as the basis for the method we used in our study, and in [25], the authors demonstrate similar height profiles of parameters within the heights from 80 to 100 km. Perhaps the described technique of atomic oxygen calculation does not work correctly above 100 km. In Figure 3, we can note that each physical parameter is decreasing after 100 km. Apparently, the simultaneous decrease in the ozone concentration, air density, and hydroxyl airglow intensity in the profiles' upper part could be the reason for incorrect performance of the above technique, resulting in the false sharp increase in the atomic oxygen concentration above 100 km. For example, the Figure 5.4 in [15] demonstrates an absence of the atomic

oxygen concentration data over 100 km. We also added the data about oxygen from the dataset described in [25] as a yellow line in Figure 4. We used the oxygen mixing ratio from dataset: [ftp://saber.gats-inc.com/Version2\\_0/SABER\\_atox\\_Panka\\_etal\\_2018\\_GRL/](ftp://saber.gats-inc.com/Version2_0/SABER_atox_Panka_etal_2018_GRL/) (accessed on 24 November 2021). and the corresponding density of the air from the SABER dataset. The averaged oxygen profile obtained for our region of interest (near FPI) had no pronounced peak, and the concentration sharply increased starting from 98 to 99 km. Possibly the data about atomic oxygen concentration from [25] are incorrect starting from the 98 to 99 km height.

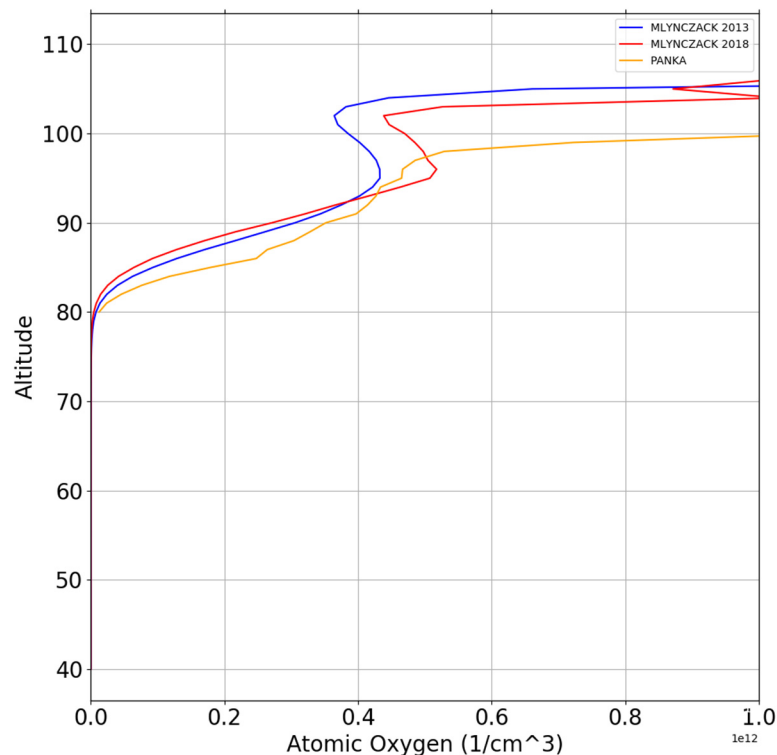


**Figure 4.** Vertical profiles of atomic oxygen concentration [ $\text{cm}^{-3}$ ]. Blue line is based on data calculated using [20], red line is calculated using [24] and yellow line is based on data from [25].

If we stretch oxygen height profiles obtained for our area of interest (near FPI) in time, we can plot 2D diagrams reflecting the seasonal behavior of the oxygen. The data prepared in such a way are presented in Figure 5. The vertical axis is the altitude, the horizontal axis is the time, and the color is the oxygen concentration. The maximum atomic oxygen concentration is observed at the heights of about 94–96 km for the top and middle panels of Figure 5. Annual variations with the maximum in August are clearly seen in the behavior of atomic oxygen time variations. In winter months, the layer with increased oxygen concentration expands and goes down to lower levels (about 85 km). In [26] it was shown that in the mid-latitudes, at the heights of 84 km, the maximum oxygen concentrations were observed in the winter. The top and middle panels of Figure 5 demonstrate how the maximum of atomic oxygen concentration moves down in winter. Such variations correspond with the movement but do not reach the heights described in the work presented in [26]. The bottom panel of Figure 5 does not contain the resolved peak height in the atomic oxygen concentration. The concentration monotonically increases with the height up to 100 km (internal limitation of the dataset), but the lower bound of the atomic oxygen layer varies here in a similar way in time as the lower bound of the atomic oxygen layer on the top panels.

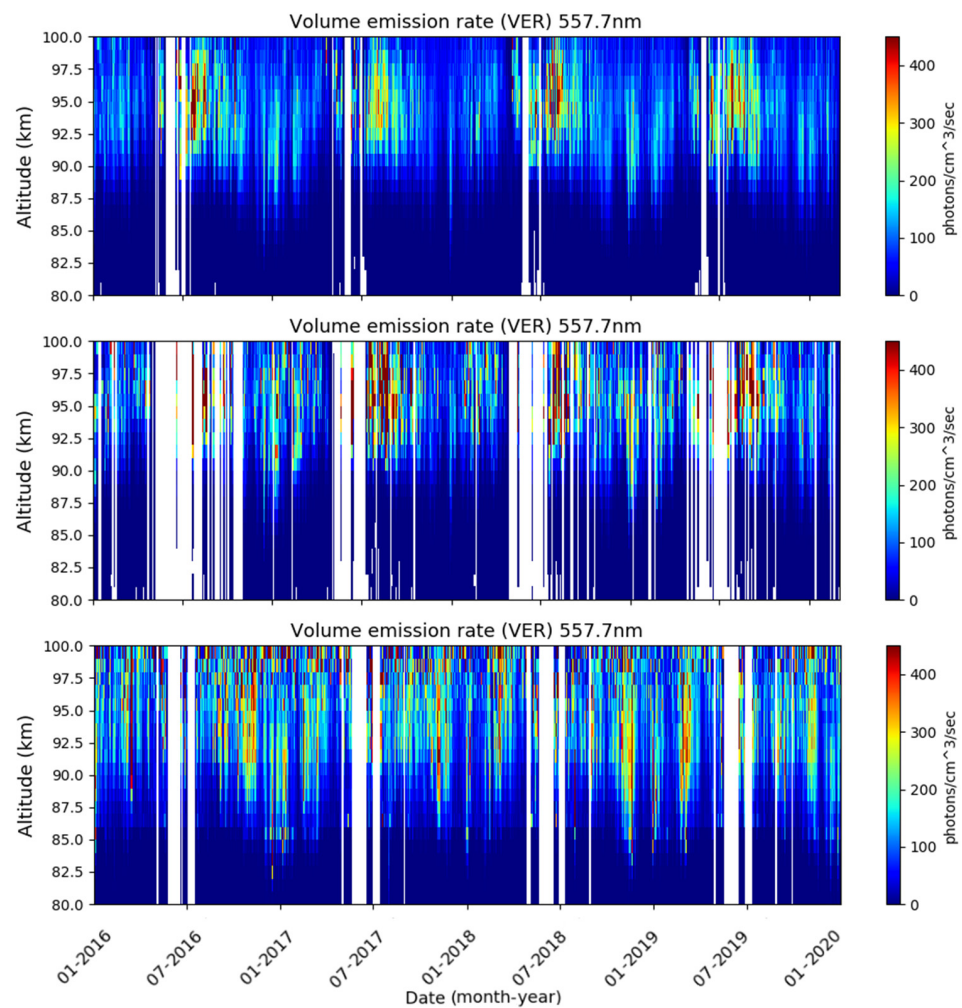


**Figure 5.** Dynamics of height profile of atomic oxygen concentration over 2016–2020 above GPO in Tory, nighttime. **Top** presents data calculated using [20]; **middle** presents data calculated using [24]; and **bottom** presents data obtained using dataset described in [25].

The same as for Figure 3, the increasing relative variability of input parameters above 100 km can be the reason for incorrect performance of the oxygen concentration reconstruction technique, resulting in the false sharp increase in the atomic oxygen concentration above 100 km. The longer gaps in data on the middle panel of Figure 5 in comparison with the top panel data are due to features of the method described in [24]. Some solutions for the quadratic equation for the oxygen concentration retrieving do not exist for the given input parameters. The longer gaps in data in the bottom panel in comparison with the top panel data are due to internal limitations of the initial dataset.

### 3. Results and Discussion

With the atomic oxygen concentration known, it is possible to calculate its intensity 557.7 nm (hereinafter 558) using the formula from [21]:

$$V_{558nm} = A_{558nm} [O(^1S)] = \frac{A_{558nm} k_1 [O]^3 [M]}{\{(A(^1S) + k_5 [O_2]) (C^{(0)} + C^{(1)} [O] + C^{(2)} [O_2])\}} \quad (7)$$

where  $M$  is the atmosphere density,  $k_1$  is the coefficient of three bodies recombination rate,  $k_5$  is the coefficient of  $O(^1S)$  extinction with oxygen,  $A_{558nm}$ ,  $A(^1S)$  are the Einstein coefficients. Values of these coefficients are presented in [21].

Figure 6 shows the airglow profiles of the 557.7 nm atomic oxygen line averaged over the entire time interval considered. The profiles were synthesized from calculated oxygen profiles data with different sets of coefficients. Here, we can note that the intensity obtained with new coefficients [24] has grown but the maximum of the airglow profile (red line) stays in the same place as the old set of coefficients [20] (green line). Similarly, the oxygen concentration intensity increases in the 93–100 km range for the new coefficients. The variance in the red curve due to a lack of data apparently has increased. The sharp increase in airglow intensity above 100 km is conditioned by the incorrectly determined atomic oxygen concentration at these heights, as was described above. The 557.7 nm airglow profile was obtained using oxygen from [25], plotted using a magenta line. One can see a very narrow peak at 97 km and then a sharp increase in the airglow intensity starting from 98 km. It is rather surprising to find a sharp resolved peak in the vertical distribution of airglow because the calculations of airglow in this case were based on the monotonically increasing atomic oxygen concentration. The peak position near the height where the methods become unstable point to some possible errors in calculations due to variable data. Nevertheless, we took this peak into account for further calculations.

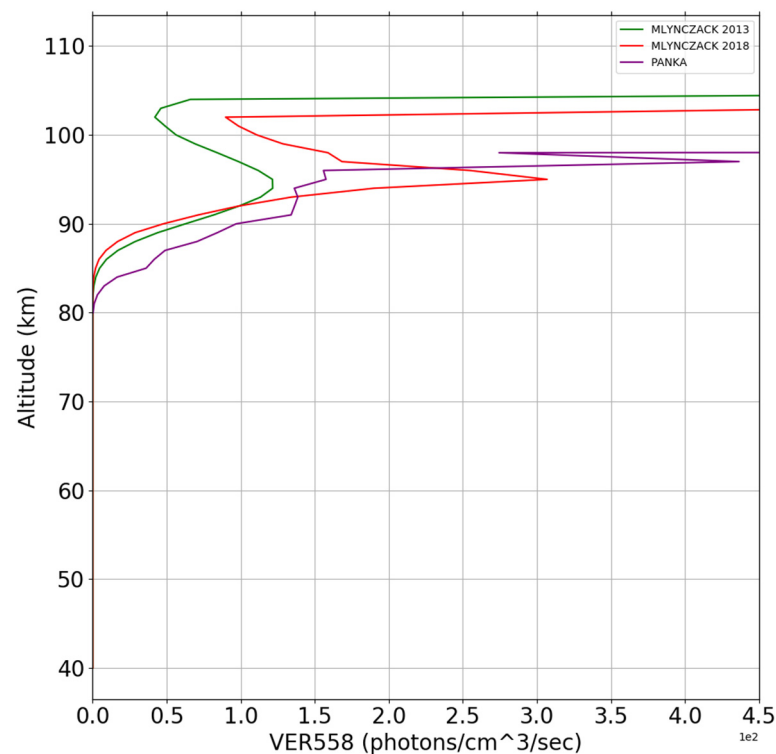


**Figure 6.** Height profiles of the 557.7 nm line airglow synthesized based on SABER data above GPO in Tory, nighttime. Integral over the entire time of observation. Green based on data calculated using [20], red line based on data calculated using [24], and magenta line based on data calculated using [25].

It can be seen that the airglow peak of the atomic oxygen 557.7 nm line is at a height of about 94–95 km. This indicates that the calculations we performed are correct in the first approximation and that the result is in agreement with the previous study [21]. In Figure 7, the temporal behavior of the 557.7 nm airglow presented in the same way as the temporal behavior of the atomic oxygen concentration in Figure 5 is shown. The top panel of Figure 7 presents data calculated using oxygen by [20], the middle panel presents data calculated using oxygen by [24], and bottom panel presents data calculated using oxygen by [25]. The main difference is the significant increase in the intensity at summer for the top and middle panels in comparison with absence of such significant seasonal intensification of 557.7 nm airglow in the bottom panel.

Worth noting is the fact that the weak variation in the airglow maximum is in antiphase with the height variation and temperature of the mesopause. The mechanism of triple collisions responsible for the formation of atomic oxygen in the state  $O(^1S)$  is inversely dependent on temperature. In this regard, the airglow maximum should follow the mesopause and be of increased intensity in summer.

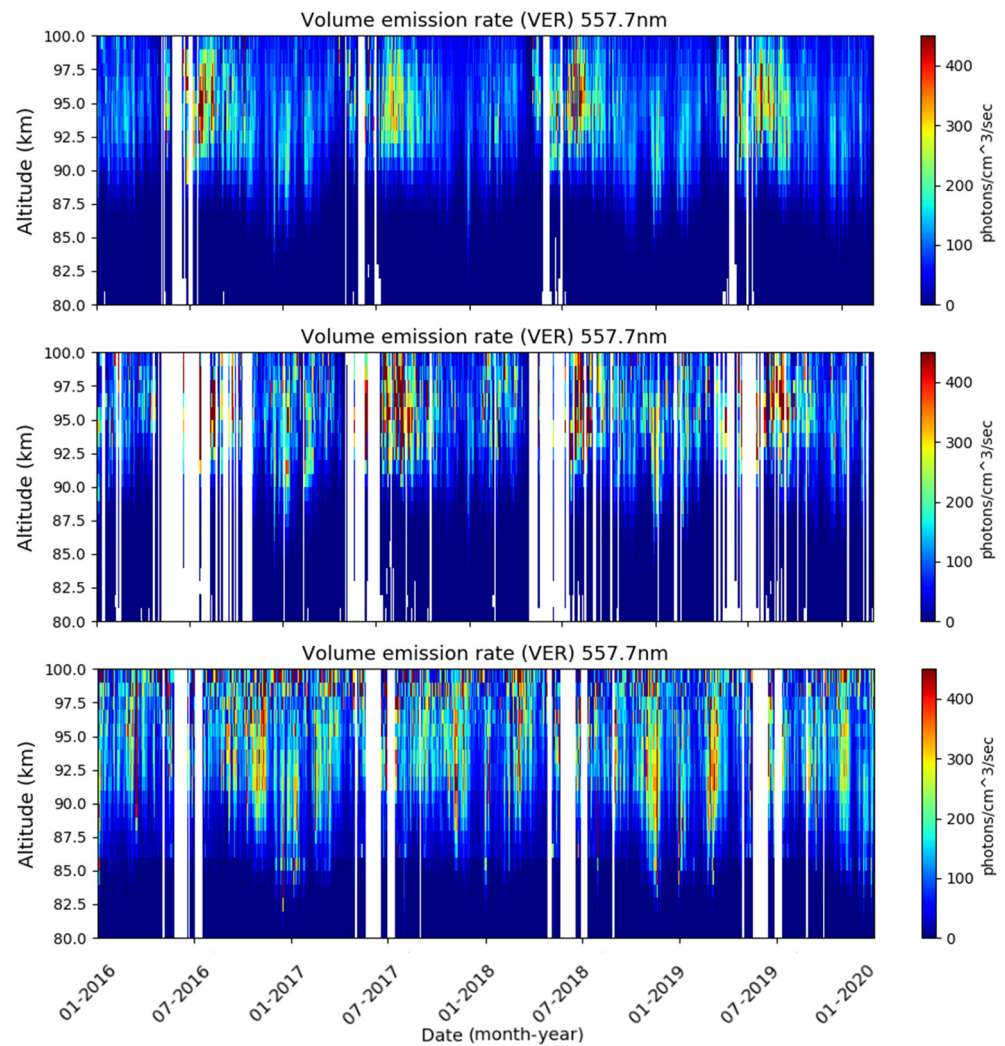


**Figure 7.** Dynamics of height profile of the atomic oxygen 557.7 nm line airglow over 2016–2020 above GPO in Tory, nighttime. **Top** panel is based on data calculated using oxygen by [20], **middle** panel is based on data calculated using oxygen by [24], and **bottom** panel is based on data calculated using oxygen by [25].

We should integrate the intensity over 80–102 km to get the correct values intensity in order to compare the ground-based and satellite observations. The 557.7 nm emission-integrated intensity obtained from SABER data and the interferometer-observed emission show a good match, especially in winter and springtime (Figure 8). The temporal behavior of integrated intensities in the bottom panel of Figure 8 already exhibit the mentioned absence of a summer increase in the 557.7 nm intensity obtained using more clear data from [25].

Here the 557.7 nm airglow intensity observed by FPI is in arbitrary units. We did not yet calibrate the intensity to bring it to the photons flux values, but we took into account the background. Thus, the arbitrary units intensity is the 557.7 nm line intensity, which should coincide rather well with the real 557.7 nm photons flux.

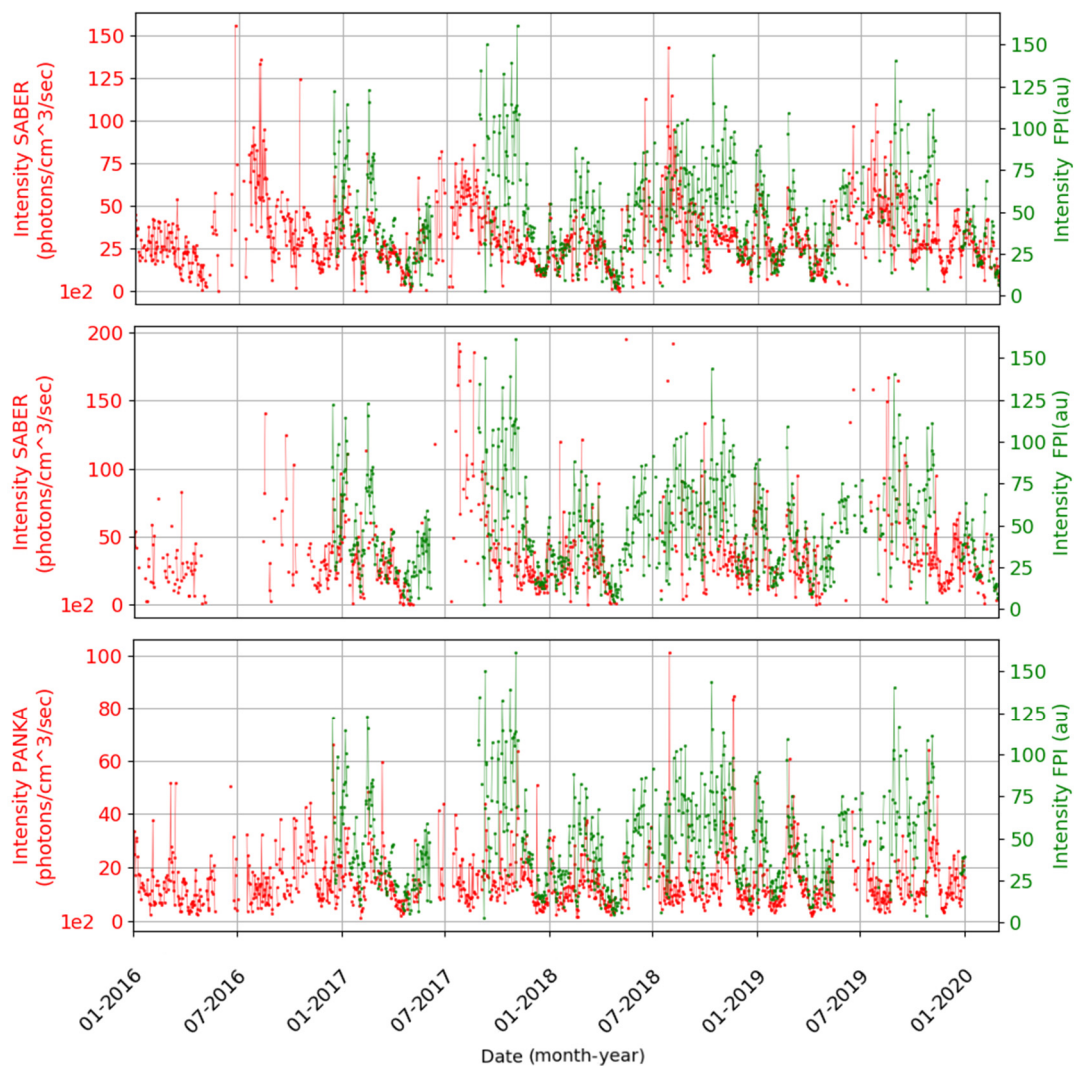


**Figure 8.** Dynamics of the 557.7 nm line intensity observed with Fabry–Pérot interferometer (green) and the 557.7 line intensity integrated in height as calculated from SABER data (red) in 2016–2020 above GPO in Tory, nighttime. The top panel presents data calculated using [20], the middle panel presents data calculated using [24], and the bottom panel presents data calculated using [25].

The height profile of the atomic oxygen airglow intensity reconstructed from SABER data allows obtaining the effective temperature using Equation (1) and comparing it with the results of ground-based observations. Figure 9 shows the behavior of these parameters throughout observations above the GPO in Tory, where the top panel presents data calculated using [20], the middle panel presents data calculated using [24], and the bottom panel presents data calculated using [25].

The change in the observed characteristics over time (Figure 9) shows that the effective temperature variations from SABER data have decreased their variance compared with the behavior of the average temperature in Figure 2, but they do not have a pronounced seasonal change, especially in the top and middle panels' data. The FPI-observed temperature has seasonal variations, which in the first approximation corresponds to the dynamics of seasonal temperature in the mesopause region. Significant differences using the method of reconstruction of the atomic oxygen profiles using [20,24] are not seen, although there are some gaps in the data when using [24]. The temperatures in the bottom panel are rather similar, but still there are some discrepancies in summer and autumn time, where the intensities also differ (see Figure 8).

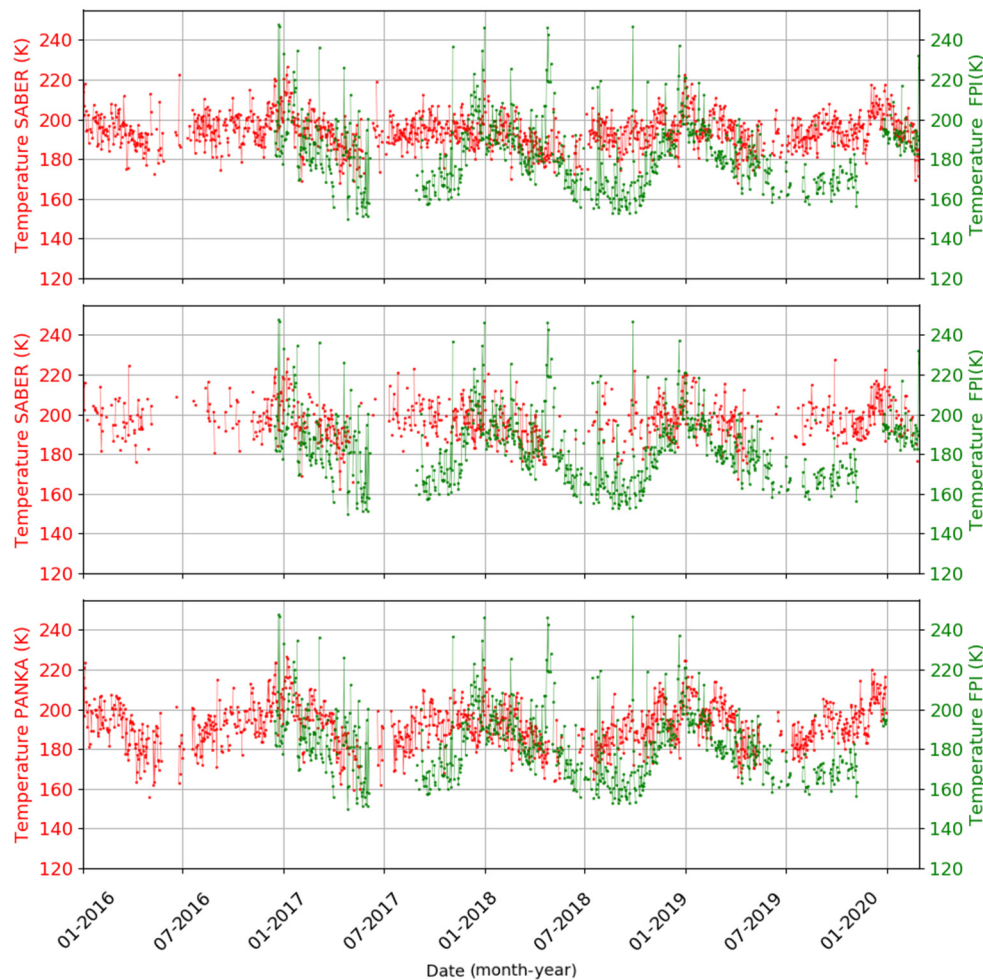


**Figure 9.** Dynamics of the temperature observed with Fabry–Pérot interferometer (green) and of the effective temperature calculated from SABER data (red) in 2016–2020 above GPO in Tory, nighttime. The top panel presents data calculated using [17], the middle panel presents data calculated using [24], and the bottom panel presents data calculated using [25].

As it was mentioned, seasonal variation in the height of the 557.7 nm intensity maximum does not correlate with the mesopause position. In this regard, let us assume that the possible reason for different seasonal variations in temperatures obtained using different methods (Figure 9) is due to our incorrect reconstruction of the  $O(^1S)$  airglow height profile using the proposed methods and SABER data. The reason can be in the incorrect height of the airglow intensity maximum. To briefly check the assumption, we used a simple technical procedure similar to the one used in [11]. By shifting vertically the airglow height profile obtained from SABER data, we calculated a new effective temperature using Equation (1) for every shift like this. To find the most appropriate new height of the airglow maximum position, we used the error weighting function that was calculated over the entire period of observation:

$$D(h) = \sqrt{\frac{\sum_i^N I_i (T_{(FPI)i} - T_{(SABER)hi})^2}{\sum_i^N I_i}} \quad (8)$$

where  $I_i$  is the atomic oxygen intensity integrated in height,  $T_{(FPI)i}$ —atmosphere temperature measured with Fabry–Pérot interferometer,  $T_{(SABER)hi}$ —atmosphere effective temperature determined from SABER/TIMED data for the profile whose maximum is the

height  $h$ , index  $i$  is the point of observation time. The height corresponding to the minimum value (Equation (8)) means that for a given position of glow profile, temporary variations in FPI-measured temperature will demonstrate the most exact coincidence with temporary variations in SABER-detected effective temperature. Figure 10 shows the error function (Equation (8)) calculated for different height shifts of the profile of atomic oxygen airglow. The error function was calculated for profiles obtained by three different methods.

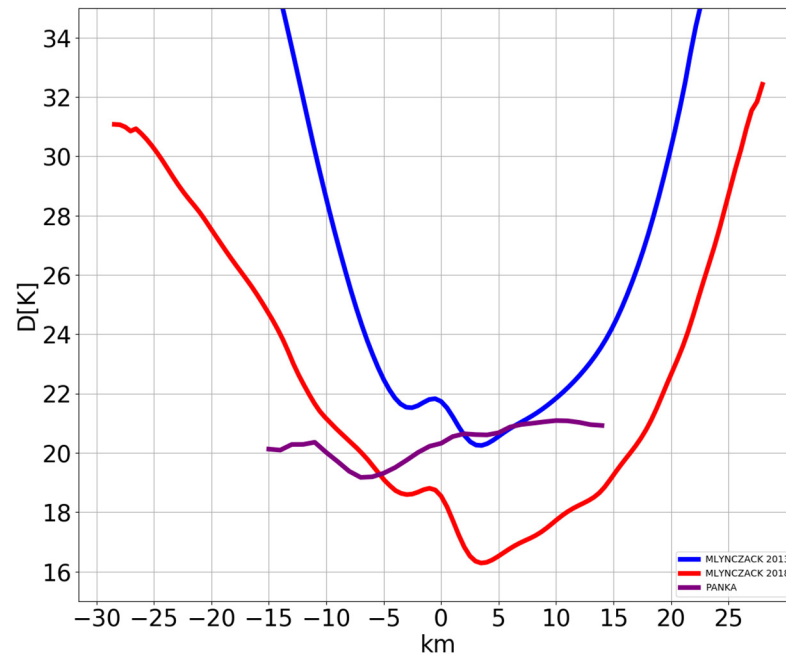


**Figure 10.** Graph of the error function dependence on airglow profile height shift. Blue is based on data calculated using [17], red is based on data calculated using [24], and magenta is based on data calculated using [25].

The minimum of the error weighting function for the blue line falls on the height shift of +2 km (~97 km) and for the red line on the height of +3 km (98 km). The height shift obtained for the magenta line is -7 km (90 km). Such a difference apparently appears from the absence of pronounced seasonal variation in the 557.7 nm intensity obtained using [25] because the essence of the described Equation (8) procedure is a minimization of the difference in seasonal variations of two raw data sets.

Seasonal behavior for the effective temperature obtained using shifted intensity height profiles matches better the behavior of the interferometer-measured temperature. In the top and middle panels of Figure 11, we put the effective temperatures calculated from airglow profiles arising from [20,24] and shifted the values corresponding to their error functions' minima (Figure 10). One can see that the only deviations in the seasonal temperature variations for FPI and SABER appear in the middle of summer and autumn. The FPI temperature here is lower than the temperature obtained using SABER data. The integrated intensities for FPI and SABER also differ at their periods (Figure 8). Intensity from FPI is higher than intensity from SABER data. Apparently this lack of additional intensity in SABER data results in the differences in the temperatures observed.

The variation in the effective temperature obtained with the shifted airglow profile by [25] is (bottom panel of Figure 11) increased, and the seasonal variations became less pronounced. It can be due to the above-mentioned difference in the shifting direction of the airglow profile. Apparently this is due to the above-mentioned absence of pronounced seasonal variations in the airglow intensity obtained by [25]. One needs to mention the fact that without shifting the effective temperature obtained using the 557.7 airglow profile by [25], the result better fits the temperature obtained by FPI (Figure 9). The airglow profile

in this case concentrates the intensity at higher altitudes in comparison with airglow profiles by [20,24]. Therefore, the reason for the similarity in temperatures in this case can again be the intensity profile placed at higher altitudes for effective temperature calculation.

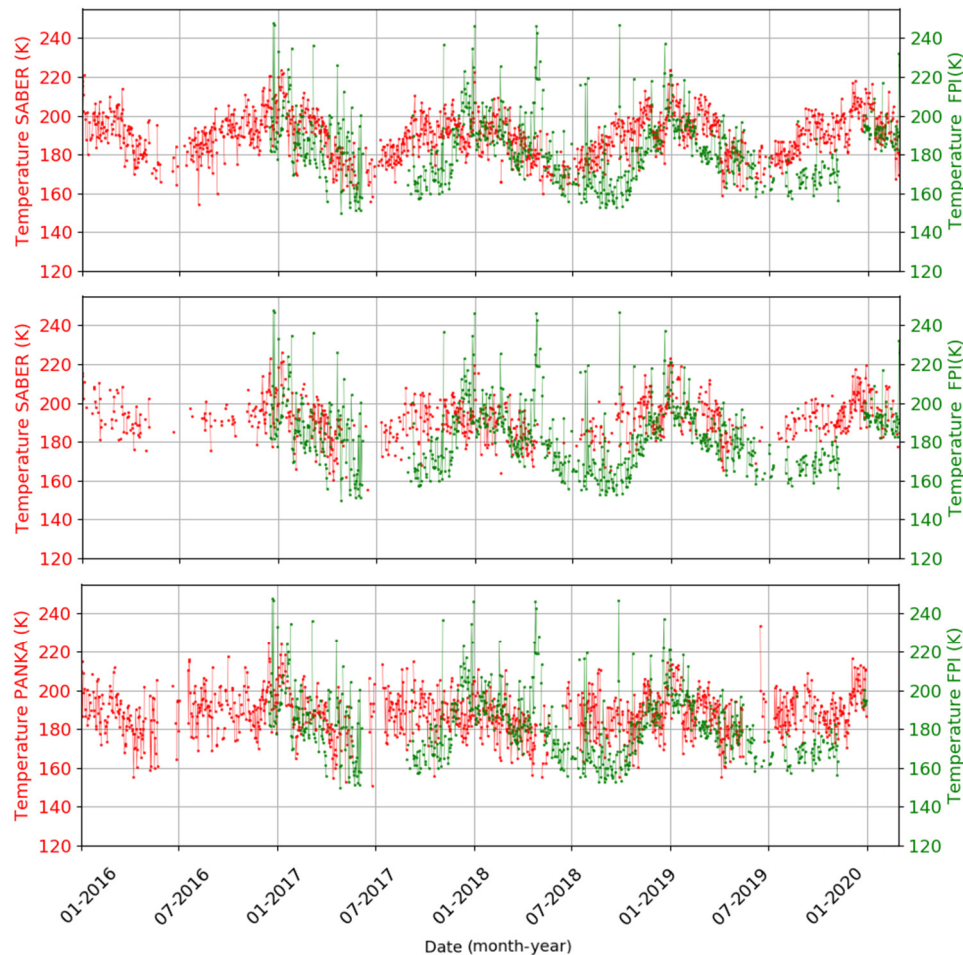


**Figure 11.** Dynamics of the temperature observed with Fabry–Pérot interferometer (green), and dynamics of the effective temperature calculated from SABER data (red) with the shift in the height of the intensity profile in 2016–2020 above GPO in Tory, nighttime. The **top** panel presents data calculated using [20], the **middle** panel presents data calculated using [24], and the **bottom** panel presents data calculated using [25].

Because it is complicated to see the details of the data in Figures 8 and 9, Figure 12 demonstrates the results using coefficients from [20] because the amount of data is larger than using coefficients from [24]. It can be mentioned that in winter–spring and in the first half of the summer period, we have better correspondences between intensity and temperature than in the last half of summer and all of the autumn period. However, should the winter period be considered in more detail, as an example, one can note that the interferometer-observed behavior of the 557.7 nm intensity coincides with the that of the intensity from SABER data, while the temperature behavior is still somewhat inconsistent (Figure 12).

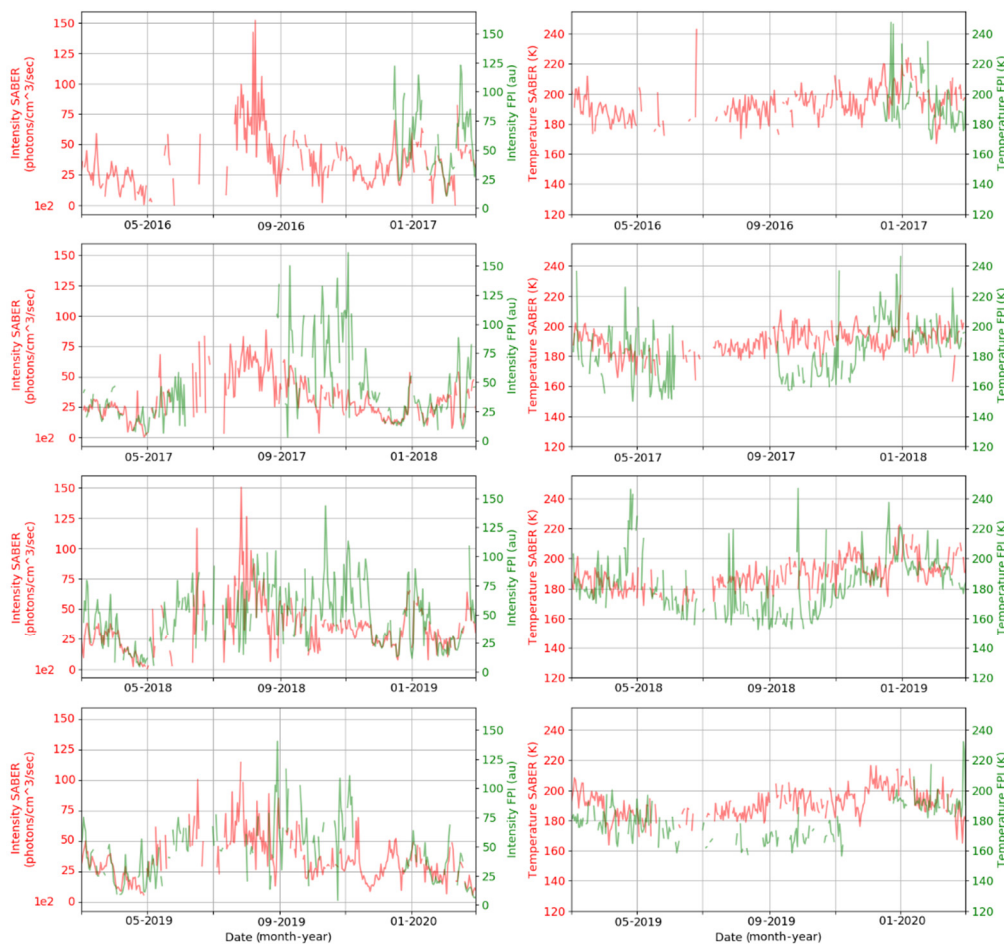


**Figure 12.** Results of intensities and temperatures comparison after the intensity peak is shifted to 97 km. **Left:** intensities, **right:** temperatures. SABER (red) and FPI (green). Presented data calculated using [20].

The obtained better agreement of seasonal temperature variations when the airglow profile synthesized from SABER data is shifted about 2–3 km up for both versions of calculated atomic oxygen airglow using [20,24] apparently means that the airglow profile determined is not quite correct, and that in fact, the 557.7 nm emission layer is higher. At least, it is fair for mid-latitudes where the FPI is located. In addition, it should be noted that local fast (non-seasonal) temperature variations obtained using the two instruments are in antiphase. Moreover, there is an inverse relationship between temperature and intensity for FPI, while for the SABER-synthesized 557.7 profile, these parameters are directly correlated [12]. Note that one can observe significant differences in the behavior of MLT (mesosphere–lower thermosphere) temperature from satellite and ground-based data during sudden stratospheric warming events, when FPI data show a considerable temperature increase, and SABER data show its decrease [12]. Thus, a possible reason for these variations can be the vertical dynamics of the 557.7 nm intensity profile, which occurs due to factors that cannot be taken into account based on SABER data. For example, a change in the atomic oxygen concentration, or in the effectiveness of the Barthes mechanism due to the arrival from the underlying atmosphere of chemical components not registered with SABER can lead both to a decrease in the number of airglow precursors and to suppression of emission itself. Additionally, one should not discard the possibility that along with the Barthes mechanism at the mesopause level, there is another mechanism generating 557.7 nm emission. The intensity of this assumed mechanism can be much lower than that of the Barthes mechanism, and the airglow profile maximum can be shifted higher.

Thus, if the glow due to the Barthes mechanism will mainly be suppressed, one begins to observe parameters of the 557.7 nm line, whose glow is generated higher. This leads to an increase in the observed temperature when the glow intensity decreases. This happens because the temperature gradient above the mesopause is positive and considerably higher than underneath. As we can see from [21], the dependence of coefficients governing the airglow is significant and inversely proportional to the temperature.

#### 4. Conclusions

In our study we compared the intensities of the atmosphere night airglow 557.7 nm and the air temperatures at the mesopause level over local part of the Earth's surface in Baikal natural territory. The data were obtained with the ground-based Fabry–Pérot interferometer and TIMED/SABER satellite instrument. Pre-comparison of the two data sets demonstrated good compliance of time variations in the mesopause temperature and in the temperature measured with the interferometer. However, taking into account the glow intensity height profile, which allows for correct comparison of data from ground- and satellite-based instruments, led to a discrepancy in the results: the effective integrated temperature calculated from the SABER parameter profiles did not reproduce the seasonal temperature variations detected with FPI. Additionally, variation in the position of the maximum of atomic oxygen airglow profile in time from SABER data did not follow the mesopause position. This was inconsistent with the recognized (Barthes) mechanism of generation of the 557.7 nm airglow, whose effectiveness becomes lower as the temperature increases.

We assumed that the emission layer height profile determined using simple astronomical models and satellite data was incorrect—namely, that the position of the calculated layer airglow maximum was wrong. Therefore, shifting this synthesized profile of intensity, whose maximum was detected at the 94 km by using [20] and 95 km by using [24] coefficients, height relative to temperature, from initial SABER data, we re-calculated the effective temperatures. The best coincidence of temperature variations obtained with ground-based and satellite instruments was achieved when the intensity maximum was shifted to the height of 97 km by using [20] and 98 km by using [24] coefficients. The coefficients according to [24] showed that the maximum atomic oxygen concentration and emission intensity were 1 km higher than the old version [20]. But using [24] we obtained less data on the concentration of atomic oxygen compared with [20]. The same comparisons performed for 557.7 nm airglow profile obtained based on [25] atomic oxygen data did not lead to the agreement in the temperatures obtained by FPI and SABER. The reason is the absence of distinct seasonal variations in atomic oxygen and in 557.7 nm airglow. However, the higher position of airglow obtained based on [25] led to rather good agreement with the temperature from FPI and the effective temperature calculated without shifting of the airglow profile in comparison with the same values calculated based on [20,24].

The shift in the emission intensity maximum according to SABER data contributed to the almost correct reconstruction of seasonal temperature variations according to SABER. However, Fabry–Pérot and SABER data demonstrated discrepancies in short-term temperature variations, especially in summer, which suggests the existence of additional factors distorting the 557.7 nm line airglow profile and requires further study. In future research, one should take into account more complicated photochemical models for green airglow, where one should pay more attention to the height of the emission maximum or double-peak structure in the resulting calculations. We also do not discard other possibilities, such as a change in the width of the emission profile, for example.

**Author Contributions:** Software, data analysis and visualization, A.S.; conceptualization, methodology and project administration, R.V.; writing—review and editing, O.Z. All authors have read and agreed to the published version of the manuscript.

**Funding:** The work was supported by the Ministry of Science and Higher Education of the Russian Federation, the grant No. 075-15-2020-787 for implementation of Major scientific projects on priority areas of scientific and technological development (the project «Fundamentals, methods and tech-

nologies for digital monitoring and forecasting of the environmental situation on the Baikal natural territory»).

**Institutional Review Board Statement:** Not applicable.

**Informed Consent Statement:** Not applicable.

**Data Availability Statement:** Satellite data SABER TIMED from <http://saber.gats-inc.com/data.php> (accessed on 24 November 2021) and ground-based Fabry-Pérot interferometer from <http://atmos.iszf.irk.ru/ru/data/fpi/archive> (accessed on 24 November 2021).

**Acknowledgments:** The results were obtained using the equipment of the Shared Equipment Center “Angara” <http://ckp-rf.ru/ckp/3056/> (accessed on 24 November 2021).

**Conflicts of Interest:** The authors declare no conflict of interest.

## References

- Cheng, X.; Yang, J.; Xiao, C.; Hu, X. Density Correction of NRLMSISE-00 in the Middle Atmosphere (20–100 km) Based on TIMED/SABER Density Data. *Atmosphere* **2020**, *11*, 341. [CrossRef]
- Parihar, N.; Singh, D.; Gurubaran, S. A comparison of ground-based hydroxyl airglow temperatures with SABER/TIMED measurements over 23° N, India. *Ann. Geophys.* **2017**, *35*, 353–363. [CrossRef]
- Gavrilyeva, G.A.; Ammosov, P.P.; Koltovskoi, I. Comparison of ground-based and satellite measurements of atmospheric temperature in the mesopause region in high-latitude eastern Siberia. *Geomagn. Aeron.* **2011**, *51*, 557–563. [CrossRef]
- López-González, M.; García-Comas, M.; Rodríguez, E.; López-Puertas, M.; Shepherd, M.; Shepherd, G.; Sargoytchev, S.; Aushev, V.; Smith, S.; Mlynczak, M.; et al. Ground-based mesospheric temperatures at mid-latitude derived from O<sub>2</sub> and OH airglow SATI data: Comparison with SABER measurements. *J. Atmos. Sol.-Terr. Phys.* **2007**, *69*, 2379–2390. [CrossRef]
- French, W.J.R.; Mulligan, F.J. Stability of temperatures from TIMED/SABER v1.07 (2002–2009) and Aura/MLS v2.2 (2004–2009) compared with OH(6-2) temperatures observed at Davis Station, Antarctica. *Atmos. Chem. Phys. Discuss.* **2010**, *10*, 11439–11446. [CrossRef]
- Liu, W.; Xu, J.; Smith, A.K.; Yuan, W. Comparison of rotational temperature derived from ground-based OH airglow observations with TIMED/SABER to evaluate the Einstein coefficients. *J. Geophys. Res. Space Phys.* **2015**, *120*, 10069–10082. [CrossRef]
- Kosch, M.; Ishii, M.; Nozawa, S.; Rees, D.; Cierpka, K.; Kohsiek, A.; Schlegel, K.; Fujii, R.; Hagfors, T.; Fuller-Rowell, T.; et al. A comparison of thermospheric winds and temperatures from Fabry-Perot interferometer and EISCAT radar measurements with models. *Adv. Space Res.* **2000**, *26*, 979–984. [CrossRef]
- Holmes, J.M.; Conde, M.; Deehr, C.; Lummerzheim, D. Morphology of evening sector aurorae in  $\lambda 557.7$ -nm Doppler temperatures. *Geophys. Res. Lett.* **2005**, *32*, 1–5. [CrossRef]
- Shiokawa, K.; Otsuka, Y.; Oyama, S.; Nozawa, S.; Satoh, M.; Katoh, Y.; Hamaguchi, Y.; Yamamoto, Y.; Meriwether, J. Development of low-cost sky-scanning Fabry-Perot interferometers for airglow and auroral studies. *Earth Planets Space* **2012**, *64*, 1033–1046. [CrossRef]
- Harding, B.J.; Gehrels, T.W.; Makela, J.J. Nonlinear regression method for estimating neutral wind and temperature from Fabry-Perot interferometer data. *Appl. Opt.* **2014**, *53*, 666–673. [CrossRef] [PubMed]
- Saunkin, A.V.; Vasilyev, R.V.; Artamonov, M.F. Comparison of the upper atmosphere temperature obtained by ground-based and satellite instruments. *arXiv* **2020**, arXiv:2011.00438.
- Zorkaltseva, O.S.; Vasilyev, R.V.; Saunkin, A.V.; Pogoreltsev, A.I. The study of temperature and night green airglow at mid-latitude in MLT during winter. In Proceedings of the SPIE 11560, 26th International Symposium on Atmospheric and Ocean Optics, Atmospheric Physics, Moscow, Russia, 12 November 2020; p. 1156081. [CrossRef]
- Zorkaltseva, O.S.; Vasilyev, R.V. Stratospheric influence on MLT over mid-latitudes in winter by Fabry-Perot interferometer data. *Ann. Geophys.* **2021**, *39*, 267–276. [CrossRef]
- Russell, J.M., III; Mlynczak, M.G.; Gordley, L.L. Overview of the Sounding of the Atmosphere Using Broadband Emission Radiometry (SABER) experiment for the Thermosphere-Ionsphere-Mesosphere Energetics and Dynamics (TIMED) mission. *Proc. SPIE* **1994**, *2266*, 406–415. [CrossRef]
- Brasseur, G.P.; Solomon, S. *Aeronomy of the Middle Atmosphere*; Atmospheric and Oceanographic Sciences Library; Springer: Cham, Switzerland, 2005. [CrossRef]
- Ignat’ev, V.M.; Nikolashkin, S.V. Dissociative line profile of the 557.7 nm [OI] sporadic emission in Auroras. *Geomagn. Aeron.* **2002**, *42*, 360–365.
- Khomich, V.Y.; Semenov, A.I.; Shefov, N.N. *Airglow as An Indicator of Upper Atmospheric Structure and Dynamics*; Springer Science & Business Media: Berlin, Germany, 2008; 740p, ISBN1 354075833X, ISBN2 9783540758334.
- Mikhalev, A. Mid-latitude aurora in solar cycles 23–24 from observations in the south of eastern Siberia. *Soln.-Zemn. Fiz.* **2019**, *5*, 80–89. [CrossRef]
- Fishkova, L.M. *Night Airglow of The Earth Mid-Latitude Upper Atmosphere*; Metsniereba Publication House: Tbilisi, Georgia, 1983; 270p.

20. Mlynczak, M.G.; Hunt, L.A.; Mast, J.C.; Marshall, B.T.; Russell, J.M.; Smith, A.; Siskind, D.E.; Yee, J.-H.; Mertens, C.J.; Martin-Torres, J.; et al. Atomic oxygen in the mesosphere and lower thermosphere derived from SABER: Algorithm theoretical basis and measurement uncertainty. *J. Geophys. Res. Atmos.* **2013**, *118*, 5724–5735. [[CrossRef](#)]
21. Gao, H.; Nee, J.-B.; Xu, J. The emission of oxygen green line and density of O atom determined by using ISUAL and SABER measurements. *Ann. Geophys.* **2012**, *30*, 695–701. [[CrossRef](#)]
22. Bates, D. Excitation of 557.7 nm OI line in nightglow. *Planet. Space Sci.* **1988**, *36*, 883–889. [[CrossRef](#)]
23. Good, R. Determination of atomic oxygen density from rocket borne measurement of hydroxyl airglow. *Planet. Space Sci.* **1976**, *24*, 389–395. [[CrossRef](#)]
24. Mlynczak, M.G.; Hunt, L.A.; Russell, J.M.; Marshall, B.T. Updated SABER Night Atomic Oxygen and Implications for SABER Ozone and Atomic Hydrogen. *Geophys. Res. Lett.* **2018**, *45*, 5735–5741. [[CrossRef](#)]
25. Panka, P.A.; Kutepov, A.A.; Rezac, L.; Kalogerakis, K.S.; Feofilov, A.G.; Marsh, D.; Janches, D.; Yiğit, E. Atomic Oxygen Retrieved from the SABER 2.0- and 1.6- $\mu\text{m}$  Radiances Using New First-Principles Nighttime OH( $\nu$ ) Model. *Geophys. Res. Lett.* **2018**, *45*, 5798–5803. [[CrossRef](#)]
26. Smith, A.K.; Marsh, D.; Mlynczak, M.G.; Mast, J.C. Temporal variations of atomic oxygen in the upper mesosphere from SABER. *J. Geophys. Res. Atmos.* **2010**, *115*. [[CrossRef](#)]